Supplemental Material for

"Electronic states with non-trivial topology in Dirac materials"

1. Experimental constraints imposed on non-local transport. In this supplement, we focus on the universal exhibition of topological order in the transport properties of ideal two-dimensional topological insulators in the most straightforward and representative form. The study of the transport characteristics of the so-called ideal topological insulator SmB_6 revealed that in the three-dimensional case the transport properties significantly depend on the geometry of samples and terminal assignments. A deviation from the universal behaviour takes place also in two-dimensional systems. It occurs due to metal droplets inside real contacts. This phenomenon can be described in terms of an additional terminal. The effect of this and other factors such as the finite width of the terminal, reflections from the internal interfaces, and other conditions on amplitudes of the transitions between current and voltage terminals was studied in several papers.

Let us clarify the role played by the contacts in the edge-state transport. First of all, we note that a contact is not a time-reversal symmetry- breaking potential that mixes counter-propagating edge states with opposite spins. Contacts are finally an electron degree of freedom reservoir that incoherently populates both edge-state channels. An ideal contact populates both edge-state channels with equal weight by injecting spin-up and spin-down electrons with equal probability. This is the origin of the additional resistance produced by the contacts. A contribution of such a dephasing reservoir into an additional longitudinal resistance can be negligible under the condition $L < L_c \sim 1/\eta$. Here L is the characteristic linear size of a contact, L_c is the dephasing length, and η is the dephasing strength of the self-energy part. Note that the self-energy should not break the time-reversal symmetry. Decoherent behaviour arises due to the existence of the dephasing reservoir with the distribution function included in the so-called lesser self-energy of the leads.

However, there are sharp dips in the conductance even for small values of ηL. They can be strong enough to completely block coherent transport at one of the edges. Therefore, even a small dephasing region can equally affect a probe terminal. The experimental value of the maximal resistance for the six-terminal device is $1/7$ instead of the theoretical prediction $1/6$. Such a result is consistent with the existence of the additional dephasing region. Dephasing regions can also exist due to an inhomogeneity of the sample. The experimental results have shown that a change in the gate voltage also affects the homogeneity of the device due to trap state charging at the semiconductor-insulator interface. This leads to an inhomogeneous potential in the gated area and to the creation of the metallic islands that exist when most of the gated regions are insulating ones.

There are two different methods to suppress the non-local transport. The

first approach is to make the device scale sufficiently small so as to induce backscattering in the channels of the edge states. Backscattering occurs when the wave functions for opposite spin orientations overlap. This happens for a device width of about 200 nm. Therefore, if the width $W1$ of the central device strip is rather large, the deviation $T_{1N}^{'}$ from the ideal value $T_{1N} = 1$ is negligibly small. The same condition $W > W_1$ for the absence of the tunneling between the edges of the individual terminal is valid for the terminal width W_1. Measurements of the non-local resistance in devices when they are in the quantum spin Hall effect states show the values expected for the nonperturbative non-local edge-state transport. The numerical simulations of the scattering matrix at the metal–topological insulator interface has confirmed the negligibly small value of $T_{1N}^{'}$ for the employed samples. The second method to suppress the edge-state contribution to non-local transport is to choose non-local configurations that imply the edge channel transport over distances longer than the inelastic scattering length. This means that the maximal number of terminals $N < N_c = L_1/(W_1 + L_2)$ can be roughly estimated as 10 for the real experimental parameters. Here L_1 is the characteristic sample size and L_2 is the distance between terminals.

2. Figures 1–3 to the section "The density of surface states" of the main text.

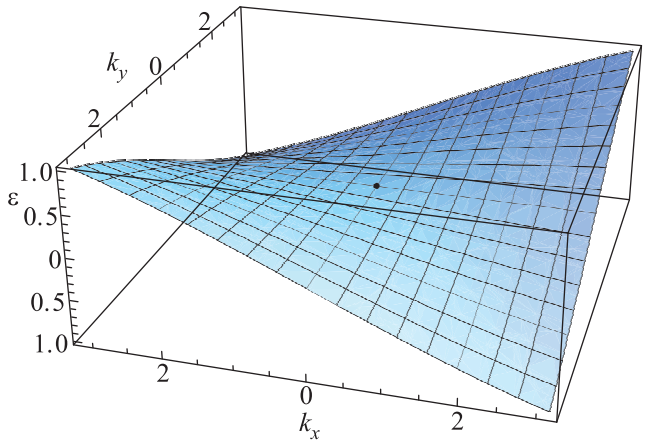

Figure 1: The spectrum of surface states in Weyl semimetal. The point denotes $k_x = k_y = 0$

3. Spin-orbit interaction in two-dimensional electron gas. We have recently studied a two-dimensional electron gas in a semiconductor heterojunction with lateral superlattice subject to a constant uniform magnetic field perpendicular to the two-dimensional plane. A typical schematic diagram of this structure is shown in Fig. 4. Spin-orbit coupling (SOC) is included in theory as Rashba and Dresselhaus terms. The magnitude of the magnetic field is chosen to correspond to a rational number of magnetic flux per unit cell of the superlattice.

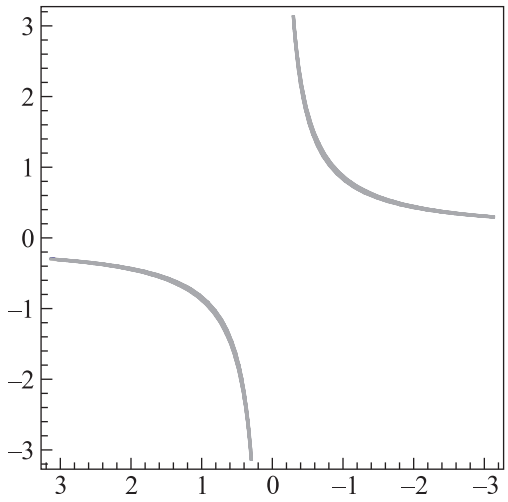

Figure 2: Fermi arcs at $\varepsilon = 0.1$

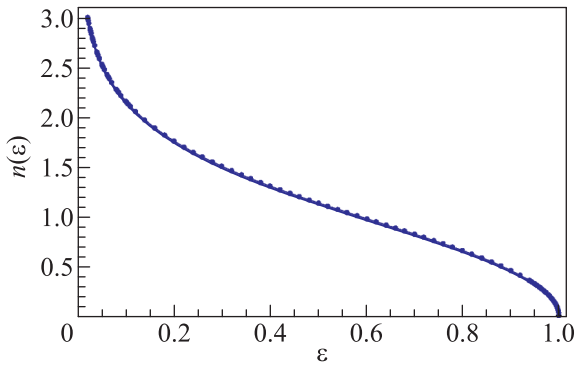

Figure 3: The density of surface states $n(\varepsilon)$ vs. the energy ε in Weyl semimetal

Model calculations are carried out in the range of experimental parameters of the system when spin, spin-orbit splitting, and splitting associated with periodic potential action on an electron are comparable. Modern artificial semiconductor superlattices are created by epitaxial growth and high-performance electron lithography. In such structures, the electron free path is much longer than the superlattice period which is of the order of tens of nanometers.

The model electron Hamiltonian can be written in the form $\hat{H} = \hat{H}_0 + V(x, y)$, where

$$\hat{H}_0 = (\hat{\mathbf{p}} - e\mathbf{A}/c)^2/2m^\star + \hat{H}_{\mathrm{SOI}} - g\mu BH\hat{\sigma}_z, \tag{1}$$

and the two-periodic function $V(x, y)$ simulates the interaction between an electron and the electrostatic field of the superlattice. Note that we considered dif-

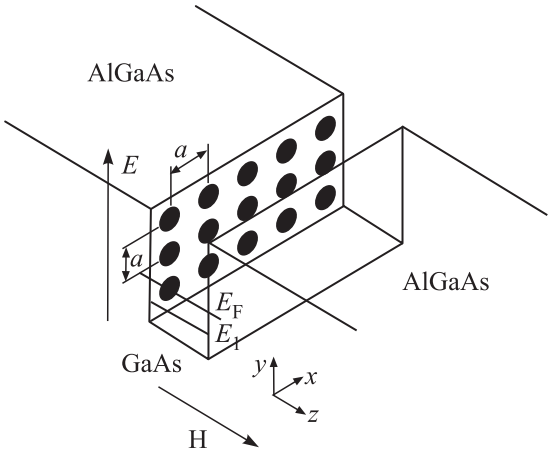

Figure 4: Schematic of a semiconductor heterojunction with a surface superlattice placed in the perpendicular magnetic field **H**

ferent cases of periodic potentials with an inversion center and without inversion symmetry. In Eq. (1), $\hat{\mathbf{p}}$ is the momentum operator, $m^\star$ is the electron effective mass, $\hat{\sigma}_z$ is the Pauli matrix, $\mu_{\rm B}$ is the Bohr magneton, g is the Lande factor, $\hat{H}_{\rm SOI}$ is the spin-orbit coupling Hamiltonian. Since the typical superlattice period of tens of nanometers is hundred times larger than the crystal period, we use the isotropic effective mass approximation at Γ-point.

In our model, the energy spectrum of an electron moving in a non-centrosymmetric potential in the presence of a perpendicular magnetic field and Rashba SOC is calculated. It is shown that for a centrosymmetric sign-constant potential, energy subbands form pairs on a certain side of non-perturbed levels. Symmetry of dispersion laws has been examined. It is shown that at a qualitative level, the photovoltaic effect can occur in the studied structures for direct transitions between states of magnetic subbands both in one pair of levels and for transitions between energy subbands of different pairs of levels with a quantum energy of the order of $\hbar\omega_c$. Here, ω_c is the cyclotron frequency. This effect is due to inversion asymmetry of the periodic potential of the superlattice.

The calculation of average values of electron spin projections in states of magnetic subbands in centrosymmetric and non-centrosymmetric model potentials of the superlattice has revealed the vortex nature of the spin distribution in the plane of the electron gas. In the case of a centrosymmetric potential, spin magnetization of the electron gas in a completely filled subband is zero. The controllable effect of non-zero spin magnetization in the plane perpendicular to the magnetic field arises because of the absence of inversion symmetry of the periodic electrostatic field of the superlattice in the presence of spin-orbit interaction in the electron gas.

The magneto-optical Kerr and Faraday effects for direct transitions between completely filled ground subband and the next magnetic subband related to

the ground spin-split Landau level are considered. The Rashba SOC in the electron gas is used. Complex Faraday and Kerr angles are calculated by the formulas obtained for a thin film of thickness $d \ll \lambda$ (λ is the incident radiation wavelength) deposited on a GaAs substrate with the static refractive index n_s:

$$\theta_{\mathrm{F}} = \frac{\sigma_{xy}}{\sigma_{xx}}\Big[1 + \frac{1}{Z_+\sigma_{xx}}\Big]^{-1}, \tag{2}$$

$$\theta_{\mathrm{K}} = \frac{\sigma_{xy}}{\sigma_{xx}^2}(-2c/d)\Big[\Big(1 + \frac{1}{Z_+\sigma_{xx}}\Big)\Big(1 + \frac{1}{Z_-\sigma_{xx}}\Big)\Big]^{-1}, \tag{3}$$

where $Z_\pm = d/[c(n_s \pm 1)]$, c is the light velocity, σ_{ij} is the conductivity tensor. The value $d = 10^{-5}$ cm corresponds to the typical thickness of a two-dimensional electron gas layer.

Fig. 5 shows the frequency dependence of the rotation angle of the polarization plane of the transmitted wave in the Faraday effect for transitions

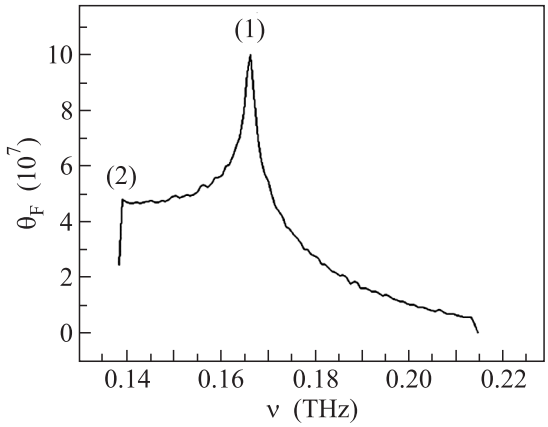

Figure 5: Frequency dependence of the Faraday angle for transitions between ground and next magnetic subbabnds in the electron spectrum of the $In_{0.23}Ga_{0.77}As/GaAs$ structure

from a ground magnetic subband to the next higher energy magnetic subband. The angle θ_{F} caused by electromagnetic wave absorption in one layer of the two-dimensional electron gas does not exceed a microradian. Note some specific features of the dependence $\theta_{\mathrm{F}}(\nu)$. We have found that peak 1 in Fig. 5 is determined by the Van Hove singularity of combined density of states in magnetic subbands. Peak 2 near the absorption edge arises only due to the spin-orbit interaction in the electron gas. The frequency of this peak corresponds to the values of the electron quasi-momentum $\mathbf{k}$ in the Brillouin magnetic zone for which z-projections of spin polarization of stationary states in the considered magnetic subbands are equal (see Fig. 6). At the frequency of this peak, the Faraday radiation ellipticity changes its sign.

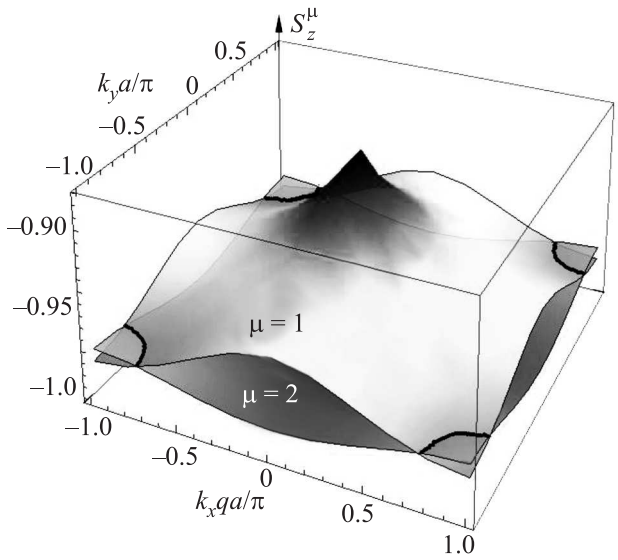

Figure 6: Spin polarization of stationary quantum electronic states in the magnetic Brillouin zone in the ground ($\mu = 1$) and next ($\mu = 2$) magnetic subbands of the spectrum. Lines of intersection of surfaces in the **k**-space in which electron states correspond to peak 2 in Fig. 2 are shown

Our calculations show that maxima of Kerr and Faraday rotation angles mainly correspond to the frequency intervals in which the longitudinal component σ_{xx} of the conductivity tensor is small, while the non-diagonal component σ_{xy} is finite, i.e., for samples in the insulator regime when external radiation induces only transverse current. The allowance for only spin splitting in the magnetic field cannot explain these features of the frequency dependences of Faraday and Kerr angles in the analysis of possible experiments with the electron gas. Therefore, along with the magnetic field, the spin-orbit interaction essentially determines the value of the circular dichroism in the lattice structures. Note that our model calculations of the magneto-optic effects in the electron gas with Dresselhaus SOC reveal qualitatively the same features of the frequency dependences of Kerr and Faraday angles.